Modeling of 3D gamma interaction position in a monolithic scintillator block with a row-column summing readout

Daniel A. B. Bonifacio, *Member, IEEE,* and Mauricio Moralles, *Member, IEEE*

***Abstract*—Current positron emission tomography (PET) systems have their detector design based on discrete scintillation crystals. Spatial resolution of these systems are directly related with the size of the crystal segments. On the other hand, cost and complexity increase considerably as the size of the crystal segments decreases. Detector design with continuous scintillator is another approach that improves the energy resolution and sensitivity without degrading the spatial resolution. In this work, we report a method to determine the gamma interaction position with depth of interaction (DOI) capability inside a monolithic crystal coupled to a photodetector array. The method is based on estimating parameters of a model which describes the signal distribution of the optical photons collected by the photodetector array in a row-column summing readout scheme. Evaluation data were simulated using the GATE framework (Geant4 Application for Emission Tomography) to characterize the detector and to compare the interaction position of the incident gamma with the position registered by the detector.**

I. Introduction

CURRENT positron emission tomography (PET) systems have their detector design based on discrete scintillation crystals. Spatial resolution of these systems are directly related with the size of the crystal segments. On the other hand, cost and complexity increase considerably as the size of the crystal segments decreases. Detector design with continuous scintillator [1], [2] is another approach that improves the energy resolution and sensitivity without degrading the spatial resolution [3]. Hence, inherent disadvantages of pixelated crystal do not exist. However, algorithms to estimate 3D gamma interaction position have to be employed. Anger logic is the most used method and provides only a 2D interaction position without depth of interaction (DOI) capability. Advances in the field of digital electronics have encouraged the development of several methods. The use of maximum likelihood method for position estimation was firstly proposed in 1976 [4] and improved later [5]. Another work [6] reports on a modied Anger logic by adding an analog resistive net to determine the light dispersion, which is directly related to DOI calculation. Anger logic was also proposed in a work that includes DOI determination capability using scintillator layers [7]. Moreover, the adoption of neural networks have already been published before [8]. Aiming to reduce the quantity of calibration procedures of the block detector, Ling and collaborators [1] proposed empirical models based on 2D functions that can be employed for position estimation: Gaussian distribution, Cauchy-Lorentz distribution and a parametric distribution, which is a generalization of Cauchy-Lorentz distribution. However, DOI estimation is performed by means of calibration. Another 3D positioning procedure [2] uses the nonlinear least squares method and does not requires a previous calibration. Albira PET scanner [9] is the only commercially available scanner that uses monolithic block detector.

In this work, we report a method to determine the gamma interaction position with DOI capability inside a monolithic crystal coupled to a photodetector array. The method is based on estimating parameters of a model that describes the signal distribution of the optical photons collected by the photodetector array in a row-column summing readout scheme. This kind of concept have been previously proposed, using both position sensitive photomultiplier tubes [1], [9], [5] and silicon photomultipliers [7], [10], however channel readout is performed individually or using a modified Anger logic. Row-column summing readout scheme provides a lower number of channels to be processed than individual readout and also presents less distortions near crystal borders than Anger logic [11]. Evaluation data were simulated using the GATE (Geant4 Application for Emission Tomography) framework [12], which is a code specific for tomographic applications based on the Geant4 toolkit [13].

II. Methods

A. PET detector design

The detector design is schematized in Fig. 1. Preliminary simulation results showed that crystal thickness cannot be larger than 10 mm, to avoid compromising the spatial resolution. The detector consists of a $28.2 \times 28.2 \times 10\,\mathrm{mm}^3$ monolithic LYSO crystal (Proteus Inc.) coupled to an 8×8 array of Micro-pixel Avalanche Photo Diode (MAPD-3N, Zecotek Photonics Inc.), which is based on the silicon photomultiplier (SiPM) technology. The crystal is polished in all faces and wrapped in Teflon. Each MAPD-3N has a sensitive area of $3 \times 3\,\mathrm{mm}^2$ and an epoxy protection layer of 0.26 mm. The array pitch is 3.6 mm wide. The optical coupling consists of a Meltmount 5870 (Cargille Laboratories Inc.) layer with 100 nm.

Manuscript received November 4, 2012. This work was supported in part by the CAPES and CNPq agencies.

D. A. B. Bonifacio was with the Institute of Physics, University of Sao Paulo, Sao Paulo, Brazil. Now is with the Institute of Radioprotection and Dosimetry, IRD/CNEN, Rio de Janeiro, Brazil (e-mail: daniel@ird.gov.br).

M. Moralles is with the Nuclear and Energy Research Institute, IPEN/CNEN, Sao Paulo, Brazil (e-mail: moralles@ipen.br).

978-1-4673-2030-6/12/$31.00 ©2012 IEEE

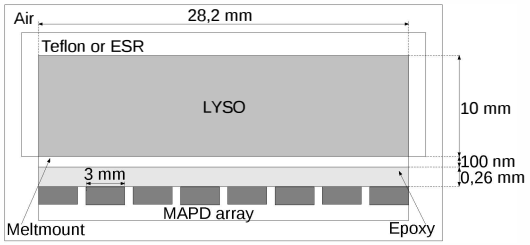

Fig. 1. Detector scheme of the simulated optical layers, volumes and materials.

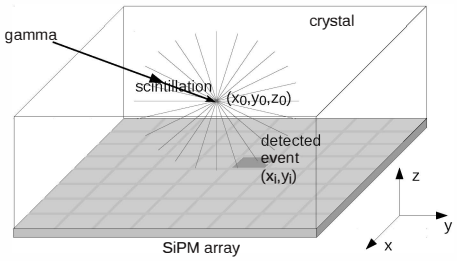

Fig. 2. Scintillation event occurring in the position $(\mathrm{x_0},\ \mathrm{y_0},\ \mathrm{z_0})$, after energy deposition by a gamma ray, and optical photon detection by an element of a SiPM array in the position $(\mathrm{x_i},\ \mathrm{y_j})$. The origin (0, 0, 0) is in the center of the SiPM array.

B. Determination of the interaction position

The interaction position of gamma radiation inside the crystal was determined using a method based on estimating parameters of a model that describes the signal distribution of the optical photons collected by the photodetector array, as shown in Fig. 2.

X and y-axes define the plane of the SiPM matrix and the position $(\mathrm{x_i},\ \mathrm{y_j})$ represents the center of one SiPM element of the matrix. The figure also illustrates the back side readout (BSR), i.e., gamma photons penetrate the scintillator crystal through the face in which SiPM matrix is coupled. Gamma photon attenuation by the SiPM matrix is considered negligible.

This method has the ability of calculating the depth of interaction $\mathrm{z_0}$ inside the crystal. The parameters of the model are the 3D position $(\mathrm{x_0},\ \mathrm{y_0},\ \mathrm{z_0})$ and background radiation, represented by a constant. Initial values for x and y positions are determined by calculating the weighted mean with outliers removal.

The assumptions of the model for the signal distribution and parameter constraints are described hereafter. The first approximation considers that optical photon absorption and scattering inside the crystal, optical resin and epoxy layers are negligible. Only reflection and refraction on the surfaces are taken into account. The model assumes that the interaction point becomes an isotropic light source when a gamma photon interacts in the scintillator crystal. Interaction point and deposited energy can be determined by means of the flux density of measured optical photons in different elements of the SiPM matrix.

The model also describes reflections on the crystal faces using three virtual sources as indicated in Fig. 3.

Two functions describe the number of detected optical photons, Nph_i and Nph_j, of the row-column summing, respectively:

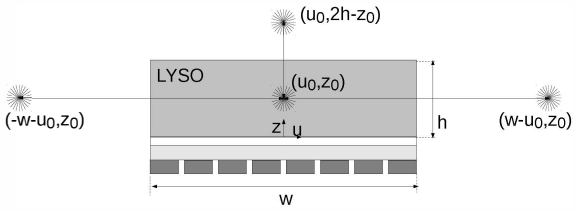

Fig. 3. Virtual sources representing reflections on the crystal faces. Virtual source positions are related with real source position.

$$Nph_i = Nph_{BG} + Nph_d(x_i, x_0, z_0) + \sum_{k=1}^{3} Nph_{vk}(x_i, x_0 + x_k, z_0 + z_k) \quad (1)$$

and

$$Nph_j = Nph_{BG} + Nph_d(y_j, y_0, z_0) + \sum_{k=1}^{3} Nph_{vk}(y_j, y_0 + y_k, z_0 + z_k), \quad (2)$$

where $Nph_d(x_i, x_0, z_0)$ and $Nph_d(y_j, y_0, z_0)$ are the sum of the signal in row and column, respectively, of optical photons that impinge directly in the SiPM matrix and are detected without suffering any reflection in the crystal. The summations of each equation describe the three virtual sources positioned at $x_0 + x_k$, $y_0 + y_k$ and $z_0 + z_k$, and represent the contribution of specular reflections on the crystal surface.

Optical photons that are not described by the previous assumptions are considered as background radiation. These optical photons have undergone at least one reflection and do not carry any information of the gamma interaction position, but they are still important to improve the energy resolution. The distribution of the background optical photons in the matrix array is considered uniform, represented by the constant Nph_{BG}.

1) Cauchy-Lorentz distribution: The inverse-square law of light intensity does not apply when the detector dimension is not negligible compared to the light source distance. Hence, the model assumes that projections onto the xz and yz planes for the distribution of optical photons emitted from the light source at position $(\mathrm{x_0},\ \mathrm{y_0},\ \mathrm{z_0})$ and impinge directly in the SiPM matrix are represented by the Lorentz-Cauchy continuous probability distribution (3) [14]

$$f_c(u; u_0, z_0) = \frac{z_0}{[(u - u_0)^2 + z_0^2]}\ , \quad (3)$$

where u is the x or y position, $\mathrm{u_0}$ is the coordinate $\mathrm{x_0}$ or $\mathrm{y_0}$ of the interaction position and $\mathrm{z_0}$ is the depth of interaction.

2) Optical photons transmission through the interfaces: The effect of light transmission through photodetector window and optical resin is described by the transmittance of a light beam depending on the incidence angle.

Reflectance and transmittance of a light beam incident on an interface separating two media with distinctive refractive indices are described by the Fresnel equations [15]. However, the block detector adopted in this work has three interfaces (crystal/resin, resin/epoxy and epoxy/silicon) and, because of that, multiple reflections can occur. These reflections can interfere in a constructive or destructive way and the Fresnel equations do not take these phenomena into account. Hence, the transfer-matrix method [16] was employed to analyze electromagnetic wave propagation through a series of layers with different thicknesses and refractive indices. The method is based on a matrix formulation of the boundary conditions in thin films using the Maxwell equations [15]. For a L layers system, the method consists in calculating the following matrix product

$$\mathbf{M} = \mathbf{M_L} \cdot \mathbf{M_{L-1}} \ldots \mathbf{M}_j \ldots \mathbf{M_2} \cdot \mathbf{M_1}, \tag{4}$$

being

$$\mathbf{M}_j = \begin{pmatrix} cos(\delta_j) & \frac{i}{\eta_j} sen(\delta_j) \\ i\eta_j sen(\delta_j) & cos(\delta_j) \end{pmatrix} \tag{5}$$

with

$$\delta_j = \frac{2\pi}{\lambda}(n_j d_j cos(\theta_j), \tag{6}$$

where n_j e d_j are, respectively, the refractive index and thickness of the layer j and

$$\eta_j = \begin{cases} \frac{n_j}{cos(\theta_j)} & \text{(parallel polarization)} \\ n_j cos(\theta_j) & \text{(perpendicular polarization)} \end{cases} \tag{7}$$

The angle θ_j is obtained from the incidence angle θ_0 using the Snell law

$$n_0 sen(\theta_0) = n_j sen(\theta_j), \tag{8}$$

where n_0 is the refractive index of the incident medium, i.e., scintillator crystal. Hence, the electrical vector $\mathbf{E_0}$ and magnetic vector $\mathbf{H_0}$ can be calculated by

$$\begin{pmatrix} \mathbf{E_0} \\ \mathbf{H_0} \end{pmatrix} = \mathbf{M} \begin{pmatrix} 1 \\ \eta_s \end{pmatrix} \tag{9}$$

where η_s is the effective refractive index of the substrate, i.e., silicon of the SiPM. The transmittance is defined by

$$T(\theta = \theta_0; \lambda) = \frac{2\eta_s}{\eta_0 \mathbf{E_0} + \mathbf{H_0}}. \tag{10}$$

Since the scintillation light is not polarized, the transmittance should be calculated for parallel (T_p) and perpendicular (T_s) polarization, and the simple mean of the two values has to be calculated:

$$\overline{T}(\theta = \theta_0; \lambda) = \frac{T_p + T_s}{2}. \tag{11}$$

Besides that, it is needed to determine the mean of the transmittance values weighted by the emission wavelength spectrum of the crystal:

$$\overline{T}(\theta) = \frac{\sum_{i=0}^{n} [\overline{T}(\theta; \lambda_i) I(\lambda_i)]}{\sum_{i=0}^{n} I(\lambda_i)}. \tag{12}$$

Table I presents the emission wavelenght spectrum, provided by the manufacturer, and the respective refractive indices, obtained from [17].

TABLE I
EMISSION WAVELENGHT (λ) SPECTRUM, PROVIDED BY THE MANUFACTURER, AND THE RESPECTIVE REFRACTIVE INDICES (n_{LYSO}), OBTAINED FROM [17]

λ_i (nm)	intensity	n_{LYSO}
395	0.1186	1.833
405	0.2290	1.833
420	0.2380	1.827
435	0.2229	1.825
475	0.1436	1.819
505	0.0293	1.811

Fig. 4 shows the set of optical layers of the chosen block detector, where a light beam is incident on an interface separating the crystal and the Meltmount resin, making an angle θ_0. The reflection angle is θ_r and the refraction angle θ_2. The values of the refractive indices and the thickness of each layer are also indicated.

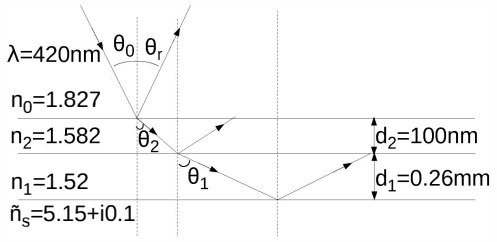

Fig. 4. Set of optical layers of the block detector and their respective values of thicknesses and refractive indices for a wavelength of 420 nm.

The matrix $\mathbf{M}$ was determined for the calculation of the optical system transmittance

$$\mathbf{M} = \begin{pmatrix} cos(\delta_1) & \frac{i}{\eta_1} sen(\delta_1) \\ i\eta_1 sen(\delta_1) & cos(\delta_1) \end{pmatrix} \begin{pmatrix} cos(\delta_2) & \frac{i}{\eta_2} sen(\delta_2) \\ i\eta_2 sen(\delta_2) & cos(\delta_2) \end{pmatrix} \tag{13}$$

An exponential function was fitted to the transmittance data, considering only incidence angles lower than the critical angle

$$\overline{T}(\theta) = a \cdot e^{b\theta} + T_0 \qquad \forall\, \theta \geqslant 0. \tag{14}$$

Equation 14 can be also represented as a function of the gamma interaction position ((u_0, z_0)) and position (u) of the collection of the optical photons by the matrix

$$\overline{T}(u; u_0; z_0) = a \cdot e^{b \arctan\left(\frac{u-u_0}{z_0}\right)} + T_0 \qquad \forall\ \arctan\left(\frac{u-u_0}{z_0}\right) \geqslant 0 \tag{15}$$

where u is the position x or y along the axis of projection concerning the intensity to be determined, u_0 is the position x_0 or y_0 of the gamma interaction at the projection axis, and z_0 is the DOI.

The fit was performed using the nonlinear least squares method (Levenberg-Marquardt algorithm); the fitted parameters are presented in table II.

TABLE II
PARAMETER VALUES FROM THE FITTED FUNCTION 15, USING THE NONLINEAR LEAST SQUARE METHOD.

Parameter	Fitted value
T_0	0.7763(6)
a	$-5.4(2.1) \times 10^{-17}$
b	0.656(7)

Fig. 5 shows the fitted curve with an angular variation from 0 to 90 degrees. The exponential function has its validity until the critical angle (56.85 degrees). Above this value, the function has negative values of transmittance, which do not have physical meaning. Hence, the model assumes the transmittance equal to zero above the critical angle.

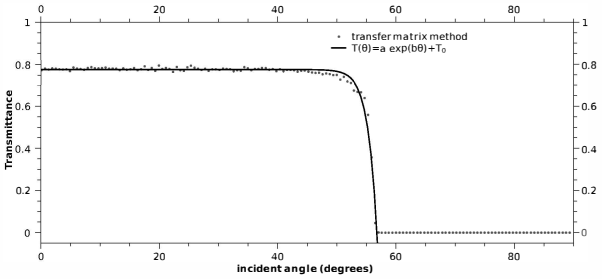

Fig. 5. Fitted curve of transmittance calculated for a light beam propagating in the epoxy and Meltmount layers as a function of the initial incident angle.

3) Signal probability distribution: Considering the model described above, the probability distribution of the the collected optical photons that impinge directly in the SiPM matrix is

$$Nph_d(u_l,u_0,z_0)=A_d \int_{u_l-\Delta u/2}^{u_l+\Delta u/2} f_c(u,u_0,z_0)\cdot \overline{T}(u,u_0,z_0)du \quad \forall\ \arctan\left(\frac{u-u_0}{z_0}\right)\geqslant 0, \tag{16}$$

where A_d is the normalization factor of the distribution and Δu is the size of the SiPM element along the corresponding axis. The defined integral takes into account the finite size of the SiPM, which are not negligible compared to the possible values of distance between the interaction point and the SiPM matrix.

As the equation 15 is valid only for incident angles larger or equal to zero ($\theta \geqslant 0$), the same condition is applied to the equation 16. However, the result can be determined for negative angles because of the symmetry of the system. The solution of the defined integral is

$$Nph_d(u_l,u_0,z_0)=A_d\left[\frac{a}{b}\cdot e^{b\arctan\left(\frac{u-u_0}{z_0}\right)} + T_0\arctan\left(\frac{u-u_0}{z_0}\right)\right]_{u_l-\Delta u/2}^{u_l+\Delta u/2}. \tag{17}$$

Defining the response function R of the element l of the SiPM matrix as

$$R(u_l,u_0,z_0)=\left[\frac{a}{b}\cdot e^{b\arctan\left(\frac{u-u_0}{z_0}\right)} + T_0\arctan\left(\frac{u-u_0}{z_0}\right)\right]_{u_l-\Delta u/2}^{u_l+\Delta u/2}, \tag{18}$$

hence

$$Nph_d(u_l,u_0,z_0) = A_d R(u_l,u_0,z_0) \tag{19}$$

Likewise, the probability distribution of each virtual source is given by

$$Nph_{v1}(u_l,u_0,2h-z_0) = A_{v1}R(u_l,u_0,2h-z_0), \tag{20}$$

$$Nph_{v2}(u_l,w-u_0,z_0) = A_{v2}R(u_l,w-u_0,z_0), \tag{21}$$

and

$$Nph_{v3}(u_l,-w-u_0,z_0) = A_{v3}R(u_l,-w-u_0,z_0) \tag{22}$$

where A_{v1}, A_{v2} and A_{v3} are the normalization factors of each distribution.

Defining

$$SumR=\sum_{l=1}^{8}\Big[R(u_l,u_0,z_0)+R(u_l,u_0,2h-z_0) +R(u_l,w-u_0,z_0)+R(u_l,-w-u_0,z_0)\Big], \tag{23}$$

the normalization factors are calculated by

$$A_d = \frac{(Nph_{total}-Nph_{BG}N_{el})\sum_{l=1}^{8}R(u_l,u_0,z_0)}{SumR}, \tag{24}$$

$$A_{v1} = \frac{(Nph_{total}-Nph_{BG}N_{el})\sum_{l=1}^{8}R(u_l,u_0,2h-z_0)}{SumR}, \tag{25}$$

$$A_{v2} = \frac{(Nph_{total} - Nph_{BG}N_{el}) \sum_{l=1}^{8} R(u_l, w - u_0, z_0)}{SumR} \quad (26)$$

and

$$A_{v3} = \frac{(Nph_{total} - Nph_{BG}N_{el}) \sum_{l=1}^{8} R(u_l, -w - u_0, z_0)}{SumR}, \quad (27)$$

where Nph_{total} is the total number of optical photons collected by the SiPM matrix and N_{el} is the number of elements of the SiPM matrix.

C. Estimation of model parameters

1) Constraints and initial values of model parameters: To avoid a convergence to the wrong point of minimum during the minimization process, it is important that the parameters to be estimated have initial values close to the real ones. Hence, an initial estimation (IE) method of these parameters was implemented and described as follow. Besides that, the inferior and superior limits of the parameters values are defined in a way to have a physical meaning and to avoid divergence of the estimates.

a) Background radiation: The initial parameter value that represents the background radiation (Nph_{BG}) is defined as the mean value of the two lower intensity signals (Nph_{low1} and Nph_{low2}) collected by the row-column summing readout:

$$Nph_{BG} = \frac{Nph_{low1} + Nph_{low2}}{2} \quad (28)$$

Inferior and superior limits are established as 50% and 100% of initial value, respectively.

b) Interaction position in the xy plane: The following algorithm was used to determine the initial values of the interaction position (x_0, y_0). The algorithm is based on a weighted mean with truncation and outliers removal, i.e., points that deviate markedly from the distribution model.

Consider i the index of the i-th signal of the n channels of the row-column readout, along the axis of position u, with i varying from 0 to $n-1$. Given all the intensity values I_i of each signal and their respective positions u_i, the following procedure was executed:

1. Determine the index of the signal with largest intensity, defined as i_{max};

2. Select all signals with intensity $I_i > 0.4\, I_{i_{max}}$;

3. Scan from $i_{max} \rightarrow n-1$ and discard all subsequent events with condition $I_i > I_{i-1}$;

4. Scan from $i_{max} \rightarrow 0$ and discard all subsequent events with condition $I_i > I_{i+1}$;

5. If the only signal which was not discarded was the one with largest intensity, then select again the previous and posterior signals relative to the largest intensity signal;

6. Compute the weighted mean of the selected signals i_s using the equation

$$\overline{u} = \frac{\sum_{i_s}(I_{i_s} - 0.4\, I_{i_{max}})u_{i_s}}{\sum_{i_s}(I_{i_s} - 0.4\, I_{i_{max}})} \quad (29)$$

Superior and inferior limits, respectively, u_{sup} and u_{inf}, were defined as

$$u_{sup} = \begin{cases} \overline{u} + \dfrac{\Delta u}{3} & \text{if } u_1 - \dfrac{\Delta u}{3} \leq \overline{u} \leq u_{n-2} + \dfrac{\Delta u}{3}; \\ \overline{u} & \text{if } \overline{u} < u_1 - \dfrac{\Delta u}{3}; \\ \dfrac{w}{2} & \text{if } \overline{u} > u_{n-2} + \dfrac{\Delta u}{3}. \end{cases} \quad (30)$$

and

$$u_{inf} = \begin{cases} \overline{u} - \dfrac{\Delta u}{3} & \text{if } u_1 - \dfrac{\Delta u}{3} \leq \overline{u} \leq u_{n-2} + \dfrac{\Delta u}{3}; \\ -\dfrac{w}{2} & \text{if } \overline{u} < u_1 - \dfrac{\Delta u}{3}; \\ \overline{u} & \text{if } \overline{u} > u_{n-2} + \dfrac{\Delta u}{3}. \end{cases} \quad (31)$$

c) Depth of interaction (DOI): Considering a front side readout, initial value and superior limit of DOI are defined as the crystal thickness value, i.e., 10 mm. Inferior limit is zero. For a back side readout, inferior and superior limit are the same as FSR, but initial value is set to zero.

D. Monte Carlo simulations

Simulations were performed using the Gate version 5.0.p1, which is based on Geant4 version 9.1.p02. With respect to the physical processes involving gamma interactions, photoelectric effect, Compton and Rayleigh scattering from Standard physical model were activated. The electron cut, given in range, was set to 30 cm to avoid secondary electron production. This value means that the secondary electron would be generated only when its range is greater than 30 cm. While scintillation is responsible for the optical photon production, the physical processes concerning optical photon interactions are optical absorption, optical Rayleigh scattering, refraction and reflection on the surfaces. Geant4 optical processes were used for this task, despite being computationally intensive [18].

III. Results

The simulations consisted of 511 keV gamma photons interacting in different positions of the crystal volume. The origin (0, 0, 0) is at the center of the SiPM array. The pitch of incident points is 2.3 mm. Because of symmetry reasons, the interaction points have x $\geq$ 0 mm and y $\geq$ 0 mm. Approximately 2,000 histories were simulated for each point of the map. The analysis of the spatial resolution of the block detector was performed by calculating the difference between the real position of the gamma interaction, obtained from the simulation input data, and the position calculated using the method described above. Contour curves of the full width at half maximum (FWHM) on the xy plane and the distribution map of the DOI (z coordinate) were calculated from the

distribution of the differences. Plots of these results, obtained for a detector with Teflon reflector and backside readout, are shown in Figs. 6 to 10.

Nonlinear Least Square (NLS) and Maximum Likelihood (ML) estimations were used to determine the model parameters. Fig. 6 shows the FWHM contour curve on xy plane for several interaction positions (POI) using the IE method. The method has a good precision to determine the position of events located far from the crystal borders. Systematic errors at the crystal borders are inherent to the method and have the same origin of those observed with the Anger logic [19], but with reduced effects due to the use of the truncated mean.

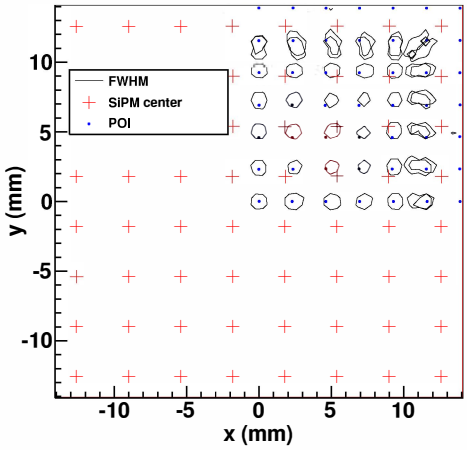

Fig. 6. FWHM contour curve for several interaction positions (POI) using IE method.

Fig. 7 and 8 shows FWHM contour curve for several interaction positions using the ML and NLS estimations, respectively. The precision to determine the position of events located far from the crystal borders is similar to the IE method, but events near the borders are registered with improved accuracy.

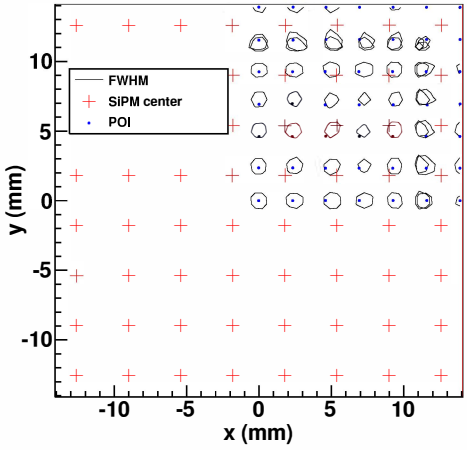

Fig. 7. FWHM contour curve for several interaction positions using the 3D method (ML estimation).

Fig. 9 and 10 exhibits DOI distribution map calculated using ML and NLS estimation, respectively, for back side readout scheme and Teflon reflector. The gray scale indicates occurring

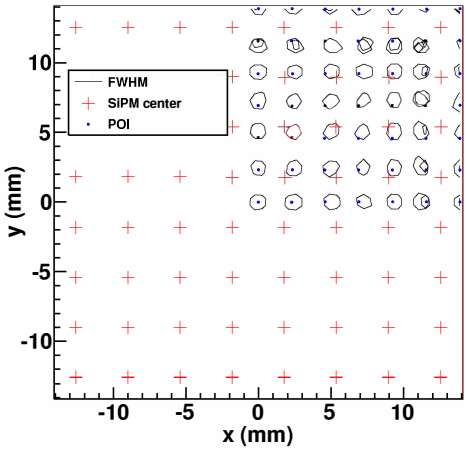

Fig. 8. FWHM contour curve for several interaction positions using the 3D method (NLS estimation).

frequency of registered events and the black crosses show the mean value of estimated DOI for each true DOI.

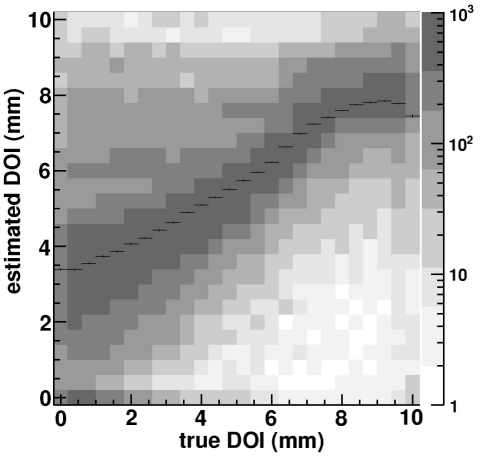

Fig. 9. DOI distribution map calculated using ML estimation.

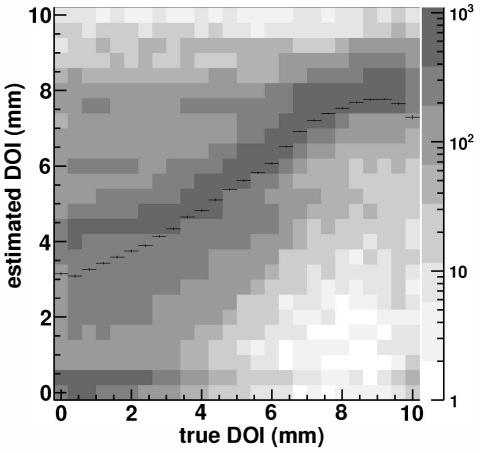

Fig. 10. DOI distribution map calculated using NLS estimation.

Distribution maps show that the DOI determination presents nonlinear distortions. The best accuracy is obtained in the

intermediate region from 4 to 6 mm. DOI values from 0 to 4 mm are overestimated; one possible reason is the fact that the model does not include position shift due to scintillation light refraction at the interface crystal epoxy resin, as illustrated in Fig. 11. This effect increases the light dispersion and produces a registered value larger than the true one.

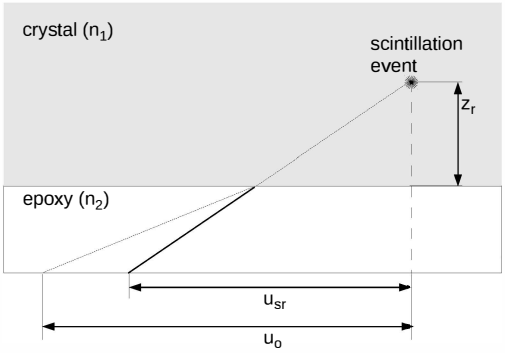

Fig. 11. Scintillation light refraction during propagation at the interface between the crystal (refractive index n_1) and epoxy resin (refractive index n_2), where $n_1 > n_2$. u_o is the position observed by the detector and z_r is the true position of scintillation event at z coordinate.

DOI values from 6 to 10 mm are underestimated. This distortion occurs mainly because the data fitting reachs a limit as light dispersion increases, and the model is not capable to distinguish clearly the background radiation from the other components. Another reason is that the model approximates a 3D real problem to a 2D solution using Cauchy-Lorentz distribution, which also implicates in some limitations.

Table III presents the standard deviation values for the calculated x, y and z coordinates relative to the real interaction position, and table IV shows the mean absolute difference values between the mean value of calculated position and its true value. Values are shown for the three estimation methods (IE, ML and NLS). Differently from an experiment, the real interaction position is exactly defined in a simulation. Hence, the standard deviation was calculated using the true value as reference, and not the mean value as would be in the case of experiments. Moreover, inherent uncertainties of the measurement process, such as mispositioning, radioactive source dimensions and angular aperture of the beam, have to be considered in an experiment. These uncertainties were not included in the simulation. The standard deviation is useful to analyze the data dispersion, and the mean absolute difference is important to quantify any shift tendency (bias) of the data distribution.

TABLE III
STANDARD DEVIATION VALUES σ_x, σ_y E σ_z OF X, Y AND Z COORDINATES, RESPECTIVELY.

method	σ_x (mm)	σ_y (mm)	σ_z (mm)
IE	2.12(1)	2.13(1)	–
ML	2.11(1)	2.10(1)	2.38(1)
NLS	2.13(1)	2.11(1)	2.51(1)

Standard deviation values vary from 2.10 to 2.13 mm on xy plane, approximately one third of a SiPM size (3 mm) and

TABLE IV
MEAN ABSOLUTE DIFFERENCE VALUES ($\overline{bias_x}$, $\overline{bias_y}$ E $\overline{bias_z}$) OF X, Y AND Z COORDINATES, RESPECTIVELY.

method	$\overline{bias_x}$ (mm)	$\overline{bias_y}$ (mm)	$\overline{bias_z}$ (mm)
IE	0.50(10)	0.50(10)	–
ML	0.39(8)	0.39(8)	1.06(17)
NLS	0.34(7)	0.34(7)	0.94(16)

from 2.38 to 2.51 mm on axis z. Mean absolute difference has values from 0.34 to 0.50 mm on xy plane and from 0.94 to 1.06 mm on axis z. Interaction position is determined with more precision and accuracy on the xy plane than on the z axis. None of the estimation methods (NLS e ML) improves the data dispersion on the xy plane, provided in the first approximation by the IE method. However, the 3D methods decrease the mean absolute difference values and include DOI determination capability. Dispersion and shift tendency of data distribution are compatible between ML and NLS, indicating that the fit quality are equivalent for both methods.

The algorithms to determine interaction position are capable to process 334 and 145 events of detected gamma per second with ML and NLS estimation, respectively, using a single core of a computer based on Intel Core i7-920 (2.67 GHz) processor.

IV. CONCLUSIONS

A method to determine the gamma interaction position inside a monolithic crystal coupled to a photodetector array was characterized and evaluated using simulated data. The proposed detector design has the potential to improve the PET technology as its performance is expected to be at least equivalent to existing systems, in addition to have a lower cost due to the employment of monolithic crystals and a row-column summing readout.

Complete system simulation should be performed to determine energy resolution, sensibility and spatial resolution at the center of field of view.

Further evaluation should be performed with experimental data in order to validate simulated results.

Despite the model considers only specular reflections on surfaces, represented by three virtual sources, results are also good for diffuse reflectors (Teflon). This owes to the fact that the main contribution for position estimation is from optical photons that impinge directly in the photodetector matrix, without suffering any reflection. However, inclusion of virtual sources in the model is important because they represent, partially, reflections related to the critical angle, which occur in all the faces of the crystal.

Distortion effects that occur in DOI determination can be reduced through several approaches. One of them would be the use of a thinner epoxy resin layer or no resin at all, to avoid at maximum optical photons shift due to refraction of light propagation through the interfaces. This implies in finding a photodetector that matches this characteristic. Another possibility to correct this effect would be a calibration

of z position, which could be performed with simulated or experimental data.

Computational efficiency analysis of the fitting method shows that ML estimation is twice as efficient as the NLS one. As spatial resolution is compatible between both methods, a decision criterion would be to choose the one which is most computationally efficient.

REFERENCES

[1] T. Ling, T. H. Burnett, T. K. Lewellen, and R. S. Miyaoka, "Parametric positioning of a continuous crystal PET detector with depth of interaction decoding," *Physics in Medicine and Biology*, vol. 53, no. 7, pp. 1843–1863, 2008.

[2] Z. Li, M. Wedrowski, P. Bruyndonckx, and G. Vandersteen, "Nonlinear least-squares modeling of 3D interaction position in a monolithic scintillator block," *Physics in Medicine and Biology*, vol. 55, no. 21, p. 6515, 2010.

[3] T. Lewellen, "Recent developments in PET detector technology," *Physics in Medicine and Biology*, vol. 53, no. 17, p. R287, 2008.

[4] R. Gray and A. Macovski, "Maximum a posteriori estimation of position in scintillation cameras," *IEEE Transactions on Nuclear Science*, vol. 23, no. 1, pp. 849 –852, 1976.

[5] W. C. Hunter, H. H. Barret, and L. R. Furenlid, "Calibration method for ML estimation of 3D interaction position in a thick gamma-ray detector," *IEEE Transactions on Nuclear Science*, vol. 56, no. 1, pp. 189–196, 2009.

[6] C. W. Lerche, "Depth of interaction enhanced gamma-ray imaging for medical applications," Ph.D. dissertation, Universidade de Valencia, 2006.

[7] S. Moehrs, A. D. Guerra, D. J. Herbert, and M. A. Mandelkern, "A detector head design for small-animal PET with silicon photomultipliers (SiPM)," *Physics in Medicine and Biology*, vol. 51, no. 5, pp. 1113–1127, 2006.

[8] P. Bruyndonckx *et al.*, "Neural network-based position estimators for PET detectors using monolithic LSO blocks," *IEEE Transactions on Nuclear Science*, vol. 51, no. 5, p. 2520, 2004.

[9] M. Balcerzyk *et al.*, "Initial performance evaluation of a high resolution Albira small animal positron emission tomography scanner with monolithic crystals and depth-of-interaction encoding from a user's perspective," *Measurement Science and Technology*, vol. 20, no. 10, p. 104011 (6pp), 2009.

[10] D. Schaart *et al.*, "A novel, SiPM-array-based, monolithic scintillator detector for PET," *Physics in Medicine and Biology*, vol. 54, no. 11, pp. 3501–3512, 2009.

[11] M. N. Wernick and J. N. Aarsvold, *Emission Tomography: The Fundamentals of PET and SPECT*, 1st ed. London: Elsevier Academic Press, 2004.

[12] S. Jan *et al.*, "GATE: a simulation toolkit for PET and SPECT," *Physics in Medicine and Biology*, vol. 49, pp. 4543–4561, 2004.

[13] S. Agostinelli *et al.*, "Geant4 – a simulation toolkit," *Nuclear Instruments and Methods in Physics Research A*, vol. 506, pp. 250–303, 2003.

[14] M. R. Spiegel, *Theory and Problems of Probability and Statistics*, 2nd ed. New York: McGraw-Hill, 1992.

[15] E. Hecht, *Optics*, 4th ed. San Francisco: Addison Wesley, 2002.

[16] Optical Society of America, *Handbook of Optics: Fundamentals, Techniques, and Design*, 2nd ed., M. Bass, Ed. New York: McGraw-Hill, 1995, vol. I.

[17] R. Mao, L. Zhang, and R. Zhu, "Optical and scintillation properties of inorganic scintillators in high energy physics," *IEEE Transactions on Nuclear Science*, vol. 55, no. 4, pp. 2425–2431, 2008.

[18] D. Bonifacio *et al.*, "A time efficient optical model for GATE simulation of a LYSO scintillation matrix used in PET applications," *IEEE Transactions on Nuclear Science*, vol. 57, no. 5, pp. 2483 – 2489, 2010.

[19] G. F. Knoll, *Radiation Detection and Measurement*, 3rd ed. NY: John Wiley & Sons, Inc., 2000.